Applied Catalysis B: Environmental 132–133 (2013) 204–211

Contents lists available at SciVerse ScienceDirect

Applied Catalysis B: Environmental

journal homepage: www.elsevier.com/locate/apcatb

Co_3O_4 nanoparticles assembled coatings synthesized by different techniques for photo-degradation of methylene blue dye

T. Warang, N. Patel, R. Fernandes, N. Bazzanella, A. Miotello*

Dipartimento di Fisica, Università degli Studi di Trento, Via Sommarive 14, I-38123 Povo, Trento, Italy

ARTICLE INFO

Article history:
Received 3 August 2012
Received in revised form 15 October 2012
Accepted 26 November 2012
Available online 3 December 2012

Keywords:
Pulsed laser deposition
Electron beam deposition
Sol–gel
Co-precipitation
Photocatalytic degradation

ABSTRACT

Co_3O_4 nanoparticles assembled coatings have been synthesized by physical (pulsed laser deposition (PLD) and electron beam deposition) and chemical (sol–gel and electroless) techniques. The morphological, structural, and optical properties of all the coatings were analyzed by SEM, XRD, Raman spectroscopy, XPS, and UV–vis spectroscopy. The catalytic activities of the several Co_3O_4 heterogeneous catalyst coatings have been compared by looking at their efficiency on degradation of methylene blue dye that occurs via photo Fenton reaction in presence of H_2O_2 or oxone oxidants. The coating synthesized by PLD exhibits the best photo-degradation rate of dye in presence of H_2O_2 (4 h) or oxone (8 min). The NPs produced by PLD process exhibit smaller average size (18 nm), narrow size distribution (σ = 3 nm), perfect spherical shape, low degree of agglomeration, and mixed amorphous-nanocrystalline phase. These special features of NPs, along with better visible light absorption, are the main factors responsible for the enhanced photocatalytic activity of the PLD Co_3O_4 NPs assembled coating. It is also observed that although the concentration of oxone (0.5 mM) was very small as compared to H_2O_2 (100 mM) the photo-degradation of MB dye solution is much faster for oxone.

1. Introduction

The textile dyes, with largest groups of organic compounds, are mainly dumped directly in the environment. These dyes are toxic to microorganism, aquatic life, and human beings, by constituting a serious concern to the ecosystem [1]. In the past, several techniques such as absorption on carbon, ultrafiltration, reverse osmosis, coagulation by chemicals, etc., have been used to separate the dye pollutants [2,3]. All these techniques are costly and require additional arrangement to remove the byproducts. On the other hand, photocatalytic degradation of organic pollutants has attracted increasing attention during the last decade as one of the promising advanced oxidation technology for the removal of organic dyes and toxic contaminants from wastewater [4]. In addition, degradation of dye by photocatalysis route produces harmless product (H_2O and CO_2) in waste water. The photo-degradation of dye occurs by oxidizing agents produced by either using TiO_2 photocatalyst, or photo-Fenton based reactions [5]. Former requires UV radiation while the photo-Fenton reaction proceeds under visible light to generate strong oxidizing agents by using oxidants such as H_2O_2, Oxone or transition metals.

Among the several transition metals studied in the past, cobalt ions (Co^{2+}) showed very good activity for photo-degradation under visible light [6]. Most importantly, cobalt catalyst shows highest activity in neutral pH. Homogeneous catalyst in form of cobalt salt solution along with oxidants is generally used to degrade dye. Ling et al. [7] compared the effectiveness of homogeneous system Co^{2+}/H_2O_2 and Co^{2+}/oxone in oxidative decomposition of basic blue 9 and acid red 183 dyes at neutral pH range. Accelerated photo-bleaching and mineralization of non-biodegradable azo-dye, Orange II, was observed using Oxone and Co^{2+} ions under visible light [8]. However, during homogeneous reaction the dissolved cobalt in the water can create further health concern and contribute to increase the pollution. Heterogeneous route of this reaction can solve the problem. Spinel Co_3O_4, containing Co^{2+} and Co^{3+} ions, has been used in advanced oxidation processes as photocatalyst for dye degradation by photo-Fenton reaction. Nanometer-scale Co_3O_4 (nanoparticles, nanorods, nanowires, etc.) displays outstanding activity and selectivity during the catalytic processes as compared to the corresponding bulk counterpart. The enhanced performance is mainly due to their large surface-to-volume atomic ratio, size- and shape-dependent properties, and high concentration of low-coordinated active surface sites [9,10]. In past, Co_3O_4 nanoparticles (NPs) have been synthesized primarily in powder form for catalysis reactions. However, in this case the major drawbacks of the catalyst are the separation after catalytic reaction, NPs aggregation, and inability to be used in conditions of continuous flow process. The separation of powder NPs catalyst from the reaction solution is so

* Corresponding author at: University of Trento, Department of Physics, Via Sommarive, 14, Povo, Trento I-38123, Italy. Tel.: +39 0461 28 1637; fax: +39 0461 28 1696.
E-mail address: antonio.miotello@unitn.it (A. Miotello).

0926-3373/$ – see front matter © 2012 Elsevier B.V. All rights reserved.
http://dx.doi.org/10.1016/j.apcatb.2012.11.040

difficult that even by centrifugation these particles remain in the solution in form of colloids. Thus, Co_3O_4 NPs deposited on suitable substrates like glass and silicon offer the best solution as green catalyst because of easy recovery and reusability. Along with the coating strategy, it is also desirable to obtain Co_3O_4 NPs with narrow size distribution and proper dispersion. In our recent work [5], Co_3O_4 NPs with narrow size distribution were successfully assembled in form of coating over glass substrate by reactive pulsed laser deposition (PLD) and optimized substrate temperature. These NPs were able to degrade dye molecules with significantly faster rate as compared to the homogeneous catalyst. In other work, Nano-sized clusters of Co_3O_4 were supported on polytetrafluoroethylene (PTFE) substrates by dip coating process and temperature of 280 °C was used to achieve good adhesion of Co_3O_4 to PTFE surface [11]. These supported Co_3O_4 NPs act as efficient photocatalyst in the fast discoloration of the azo-dye Orange II under simulated solar radiation in the presence of oxone [11].

Co_3O_4 NPs assembled-thin coatings on stainless steel, silicon, and nickel substrates have been synthesized by several techniques, such as PLD [9,10,12], electron-beam deposition (EBD) [13,14], atomic layer deposition (ALD) [15], plasma-enhanced chemical vapor deposition (PECVD) [16], and sol–gel method by dip coating [17]. In the past, Co_3O_4 coatings prepared by PLD in a temperature range of 300–600 °C possesses NPs with average size of 40–150 nm on the surface [9,10,12]. Polycrystalline Co_3O_4 thin films with grain sizes below 50 nm have been prepared by EBD and subsequent annealed in air [13] and oxygen [14] at different temperatures. Co_3O_4 thin films were synthesized by remote plasma ALD process by using the combination of cobaltocene ($CoCp_2$) as the cobalt precursor and O_2 plasma as the oxidant source [15]. CVD technique used for depositing Co_3O_4 thin films make use of Co-based organo-metallic compounds as precursor which are responsible for the presence of carboxyl groups and alcohol contents in the films along with nanoparticles (40 nm) of Co_3O_4 [16]. Švegl et al. [17] reported the synthesis of spinel Co_3O_4 thin films, with average crystallite size in the range of 20–40 nm, by using the sol–gel process with dip coating technique and annealing treatment at 300 °C and 500 °C. Chemical methods like co-precipitation and sol–gel techniques employ surfactants to prevent the agglomeration of NPs [18].

Previous different methods were able to blend Co_3O_4 NPs assembled coatings: here we make a comparison between the different synthesis techniques in connection to the efficiency in catalytic reaction of the Co_3O_4 nanostructures by highlighting strengths and limitations of the experimental techniques. Specifically, we report on the synthesis of Co_3O_4 NPs assembled thin coatings by different physical (PLD and EBD) and chemical (sol–gel and electroless) methods. The catalytic activity of these Co_3O_4 NPs assembled thin coatings as heterogeneous catalyst was tested in degradation of methylene blue dye solution via photo Fenton reaction in presence of H_2O_2 or Oxone. The detailed analysis of both the physical-chemical properties and photocatalytic efficiency show that Co_3O_4 NPs synthesized by laser ablation process possess the required morphology and structure to enhance the photo-catalytic activity.

2. Experimental

2.1. Chemicals

Cobalt chloride ($CoCl_2$), cobalt acetate tetrahydrate ($(CH_3COO)_2Co\ 4H_2O$), ammonia solution (NH_3) and ethylene glycol ($HOCH_2CH_2OH$) used for the synthesis of catalyst was obtained from Sigma Aldrich and used without any further purification. Chemicals used for photo-degradation measurements such as methylene blue (MB) dye, hydrogen peroxide (H_2O_2) and oxone ($2KHSO_5\ KHSO_4\ K_2SO_4$) were purchased from Alfa Aesar.

2.2. Catalyst preparation

2.2.1. Co_3O_4 powders

Diluted ammonia solution (25%) was added as a precipitator to the homogeneous 0.04 M aqueous solution of $CoCl_2$ under continuous stirring. After stirring at room temperature, the obtained cobalt hydroxide ($Co(OH)_2$) precipitate was filtered and subsequently washed with distilled water and ethanol. Finally, the $Co(OH)_2$ precipitated was vacuum dried and thermally decomposed at 400 °C for 2 h to obtain the Co_3O_4 powder.

2.2.2. Co_3O_4 coatings

Co_3O_4 thin coatings were synthesized by using four different methods, namely: (1) PLD, (2) EBD, (3) sol–gel method, and (4) electroless deposition.

Pulsed laser deposition: PLD was carried out, by using a pure Co target, under oxygen gas pressure in the deposition chamber. Details of the deposition apparatus are reported in Ref. [19]. The PLD chamber was evacuated up to a base pressure of 2×10^{-6} mbar prior to deposition under oxygen gas atmosphere. NPs assembled thin coatings were deposited on Si and glass substrates by using a KrF excimer laser (Lambda Physik) at operating wavelength of 248 nm, pulse duration of 25 ns and repetition rate of 20 Hz. O_2 gas pressure of about 4.5×10^{-2} mbar and substrate temperature of 150 °C was maintained in the chamber during deposition. The substrate temperature and laser energy fluence (3 J/cm^2) were chosen as in Ref. [5] where Co_3O_4 NPs synthesis by using these parameters produce maximum photocatalytic activity.

Electron beam deposition: The cobalt oxide thin coatings were prepared by EBD using Co_3O_4 pellets as source. The chamber was evacuated up to a base pressure of 2×10^{-7} mbar prior to deposition. The rate of deposition was maintained at 0.5 Å/s. The cobalt oxide coatings were deposited on glass and silicon substrates maintained at room temperature during the deposition. The as deposited coatings were annealed in static air at 400 °C for 2 h to obtain crystallization.

Sol–gel method: Co_3O_4 thin coatings were deposited on silicon and glass substrates by spin coating. To synthesize sol, cobalt acetate solution, (0.7 M) in methanol, was added to ethylene glycol solution and then the mixture was stirred for 30 min at room temperature in order to achieve a complete dissolution of the metal salt. This sol was later spun for 30 s at 2000 rpm on glass and silicon substrate using a SPS photoresist spinner, model EC 101D. The bluish thin coatings were further baked at 140 °C for 1 h. After drying, the coatings were heat treated in static air at 400 °C for 2 h to obtain crystalline Co_3O_4.

Electroless deposition: Square specimen (21 mm × 26 mm) of stainless steel (SS) substrate was ultrasonically cleaned with acetone followed by NaOH solution to remove soaks, lubricants, and finger prints. The surface of specimen was deoxidized and activated by dipping in HCl solution for 2 min and then washed with distilled water and dried at 323 K in N_2 atmosphere. Activated stainless steel substrates were dipped in a chemical bath consisting of 0.04 M aqueous solutions of cobalt(II) chloride ($CoCl_2$). The 25% diluted ammonia solution was added as a precipitator to the above chemical bath under continuous stirring. The as deposited stainless steel substrate composed of $Co(OH)_2$ film was further decomposed at 400 °C for 2 h to obtain the final crystalline Co_3O_4. For the measurement of UV–vis spectra of Co_3O_4 coatings deposited by electroless method, activated glass substrates were used for deposition. The surface of glass substrate was made rough by treating it initially in dilute hydrofluoric acid and then glass surface was activated by treatment in dilute sodium hydroxide solution. The electroless

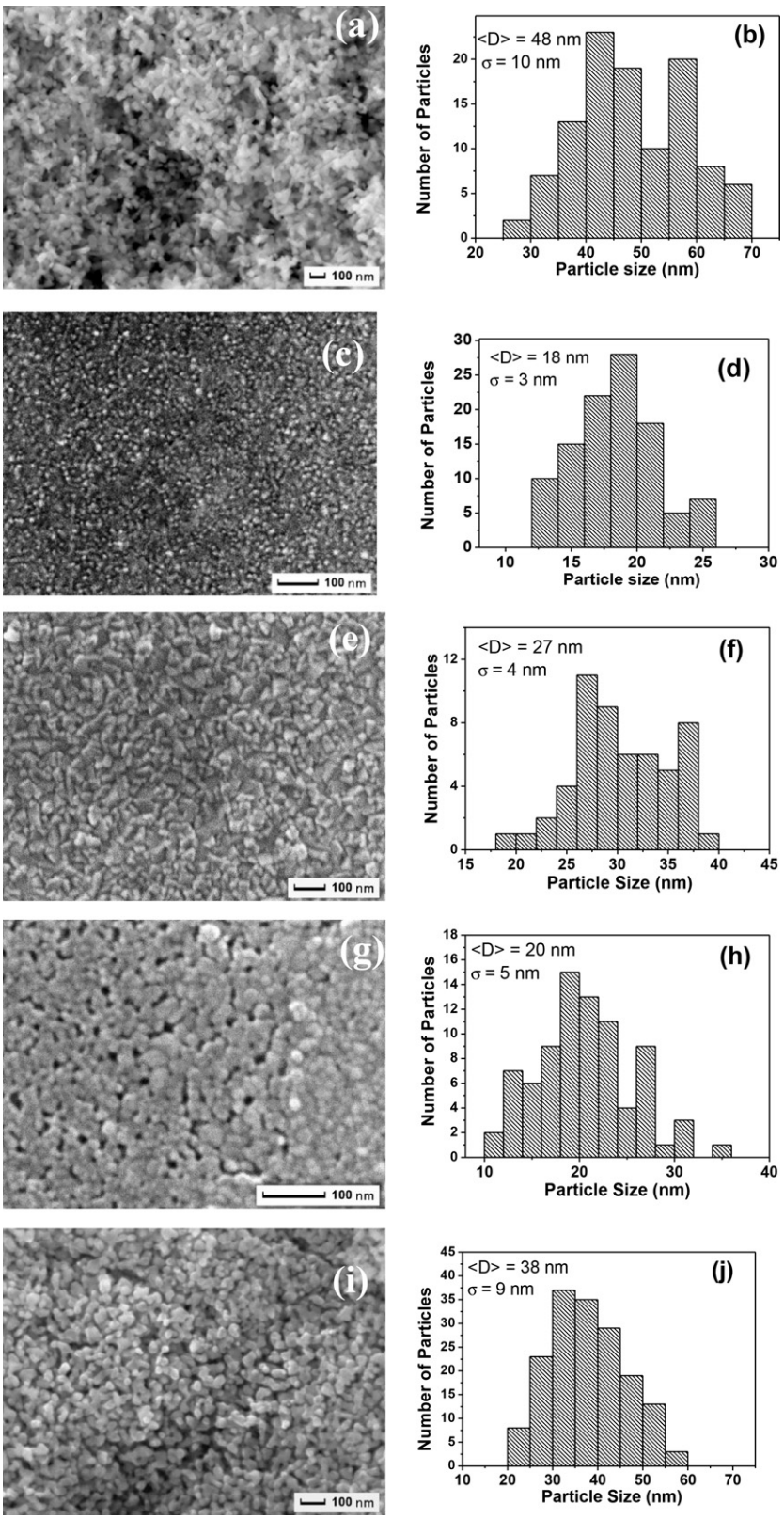

Fig. 1. SEM micrographs of the Co_3O_4 catalyst in form of: (a) powder, and coatings synthesized by (c) PLD, (e) EBD, (g) sol–gel, and (i) electroless deposition. Corresponding histogram of particle size distribution are shown in (b), (d), (f), (h), and (j).

deposition on these activated glass substrates was carried out as mentioned above.

2.3. Catalyst characterization

The surface morphology of all samples was studied by scanning electron microscope (SEM-FEG, JSM 7001F, JEOL) equipped with energy-dispersive spectroscopy analysis (EDS, INCA PentaFET-x3) to determine the composition of the samples. The structural characterization of the deposited samples was carried out by conventional X-ray diffraction (XRD), Cu Kα radiation (λ = 1.5414 Å), in Bragg–Brentano (θ–2θ) configuration. Raman spectra were recorded by using HORIBA Jobin Yvon Lab RAMAramis Raman spectrometer with diode pumped solid state laser at 532 nm. X-ray photoelectron spectra (XPS) were acquired using a Kratos AXIS Ultra^{DLD} instrument equipped with a monochromatic Al K_α (1486.6 eV) X-ray source and a hemispherical analyzer. No electrical charge compensation was required to perform XPS analysis. Optical measurements of the Co_3O_4 coatings were performed using a VARIAN Cary 5000 UV–vis–NIR spectrophotometer with normal incidence of the incoming beam. To obtain the absorbance spectra of samples deposited on glass slides, the measurements were performed in the photon energy range between 1 eV and 4.5 eV.

2.4. Photocatalytic activity measurement

Photocatalytic activity of all the Co_3O_4 powder and coatings catalyst deposited with different methods was tested by degradation of dye molecules. 50 ml of 2 mg/L MB solution was used as the dye solution. All Co_3O_4 catalysts prepared by different methods were dipped in MB solution and stirred in dark for 30 min to establish adsorption equilibrium between the solution and the catalysts. The weight of the Co_3O_4 catalyst coatings was always maintained same (1.2 mg) over constant area of the substrate. 100 W tungsten halogen lamp with visible light spectrum was used as the light source for the photocatalytic reaction. The degradation of dye was conducted using oxidizing agents in form of H_2O_2 or oxone with concentration of 100 mM or 0.5 mM respectively. After established time intervals, 1 ml MB aqueous solution was filtered out from the reactor vessel. The UV–vis adsorption spectra of the filtered solution were measured using a VARIAN Cary 5000 UV–vis–NIR spectrophotometer, and the concentration of the MB aqueous solution was estimated by analyzing the intensity of the absorption peak at a wavelength 664 nm. All the photocatalysis experiments were performed at room temperature and the pH of the solution was measured neutral during all the photocatalytic measurements.

3. Results and discussion

SEM images of Co_3O_4 powder prepared by co-precipitation method, and coatings synthesized by different methods are presented in Fig. 1. The average particles size of all the catalysts was established from SEM images by using image-analysis software. Data are summarized in Table 1 while the corresponding histograms of particles size distribution are illustrated in Fig. 1. The image of Co_3O_4 powder (Fig. 1a) shows particle like morphology with irregular shape and average size of 45 nm (Table 1). However, these particles are in agglomerated state with relatively broader size distribution (Fig. 1b). Few particles are observed in form of cylindrical nano-rods with diameter of 50 nm and length of around 100 nm. On the contrary, the surface of Co_3O_4 coating synthesized by PLD on silicon substrate (Fig. 1c) is composed of well-defined circular-shaped NPs with average size of 18 nm (Table 1) and narrow size distribution (Fig. 1d). These particles are well separated and densely arranged on the substrate surface with very low degree of agglomeration. Cross-section SEM of these coatings showed that

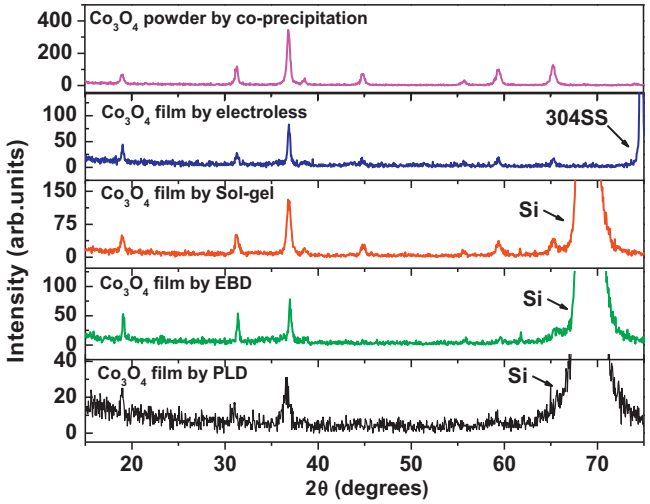

Fig. 2. X-ray diffraction pattern of Co_3O_4 catalyst powder and coatings synthesized by PLD, EBD, sol–gel, and electroless deposition.

the NPs are partially embedded on the catalyst (glass substrate) surface forming 3D structure. The NPs are formed by high laser fluence induced phase explosion phenomena [20]. Here, the irradiated target material reaches temperature of ~0.9T_c (T_c is thermodynamic critical temperature) causing a very high homogeneous nucleation of vapor bubbles below the target surface. The target surface then makes a rapid transition from superheated liquid to a matrix of vapor and liquid nano-droplets, which leave the irradiated target surface and get deposited on the substrate in form of NPs [20,21]. Oxidation mainly occurs during liquid nanodroplets flight from irradiated target to the substrate.

Fig. 1e shows the SEM image of surface of the Co_3O_4 coating prepared by EBD on silicon substrate and subsequent annealing. As deposited coating, before heat treatment shows flat surface without any structure as confirmed by SEM (figure not shown). While compact granules of irregular shape are observed on the surface of heat treated coatings. These grains are randomly oriented and separated by well defined boundaries. The grains size is distributed in narrow range (25–40 nm) (Fig. 1f) with average size of 27 nm. Due to the thermal evaporation process, vapor of atoms condense on the substrate with random orientation. After the heat treatment at 400 °C for 2 h in air, the Co_3O_4 phase crystallizes to form nano-grains.

The surface of spin coated Co_3O_4 coating on silicon substrate after annealing, as observed by SEM, is in form of assembled NPs having circular shape (Fig. 1g). The average particles size is 20 nm with uniform size distribution (Fig. 1h) but there is a clear tendency of agglomeration to minimize surface energy. A few number of voids is also observed on the surface of this spin coated coating.

The morphology of the Co_3O_4 coating produced over SS substrate by electroless deposition (Fig. 1i) is quite similar to that obtained with Co_3O_4 powder prepared by co-precipitation method (Fig. 1a). This is clearly attributed to the similarity in the synthesis techniques where NH_3 is used as the precipitator. Irregular-shaped particles are observed with average size of 38 nm and broad size distribution (20–60 nm) (Fig. 1j) as compared to coatings synthesized by other techniques.

Fig. 2 shows the XRD pattern of Co_3O_4 powders and coatings synthesized with different methods. Diffraction peaks detected at 19.0°, 31.2°, 36.5°, 38.4°, 44.8°, 55.6°, 59.0° and 65.2°, in XRD spectra of Co_3O_4 powder, prepared by co-precipitation method, are assigned to the spinel type cubic structure of Co_3O_4 with Fd3m space group [22]. These diffraction peaks correspond to the reflection (1 1 1), (2 0 0), (3 1 1), (2 2 2), (4 0 0), (4 2 2), (5 1 1) and (4 4 0), respectively. Similar diffraction peaks with lower intensity

Table 1
Crystallite size calculated from the (3 1 1) XRD peak by using the Scherrer's formula and width (FWHM) of Raman bands A_{1g} for Co_3O_4 NPs assembled coatings deposited by physical and chemical methods. The width of Raman bands A_{1g} of proper crystalline Co_3O_4 is 6.2 cm^{-1} [23].

Co_3O_4 catalyst coatings preparation technique	Crystallite size from XRD (nm)	Mean particle sizes from SEM (nm)	FWHM of Raman bands A_{1g} at 694 cm^{-1}
PLD	25	18	12.0
EBD	29	27	10.2
Sol–gel	36	20	8.3
Electroless deposition	59	38	7.1
Co_3O_4 powder by Co-precipitation method	47	48	6.4

is observed for the Co_3O_4 coatings deposited by chemical method (sol–gel and electroless) indicating well-crystallized cubic structure of Co_3O_4. However, only three peaks at 19.0°, 31.2° and 36.5° assigned to cubic Co_3O_4 are observed for coatings deposited with physical methods and these peaks are broader as compared to the other Co_3O_4 coatings. This indicates that these coatings are composed of mixed amorphous-nanocrystalline phase. The crystal sizes of all Co_3O_4 catalysts were calculated from the (3 1 1) peak using the Scherrer formula to establish the crystalline degree: data are summarized in Table 1. The crystallite size of the Co_3O_4 powders and coatings prepared by chemical methods is bigger than that of the Co_3O_4 synthesized by physical methods. No diffraction peaks are observed in the XRD spectra attributed to metallic Co or to other cobalt oxides. This means that the deposited cobalt oxide consists only of cubic Co_3O_4.

Raman spectra are presented in Fig. 3 for all the Co_3O_4 catalysts. The powder and coatings prepared by chemical methods on silicon and SS substrate by sol–gel and electroless, respectively, clearly display four bands, located at approximately 485, 525, 626, and 694 cm^{-1}, that correspond to the E_g, F^1_{2g}, F^2_{2g}, and A_{1g} modes, respectively. This suggests complete crystallization of the Co_3O_4 phase [23]. The physically deposited (PLD and EBD) Co_3O_4 coatings on silicon substrates show only three bands at 485, 525, and 694 cm^{-1} with low intensity and broad feature as compared to chemically prepared Co_3O_4 catalyst. The width of Raman peaks gives the idea of the crystalline degree of the material. The FWHM value of Raman band A_{1g} (Table 1) is higher for the Co_3O_4 coatings deposited by the physical methods (PLD and EBD) indicating mixed amorphous-nanocrystalline structure in these coatings. On the contrary, the FWHM value of the chemically prepared (sol–gel and electroless) coatings is quite close to the value reported for crystalline Co_3O_4 [23]. No vibrational modes due to impurities were detected. This result is in good agreement with XRD results.

XPS spectra of Co_{2p} and O_{1s} core levels of Co_3O_4 powders and coatings synthesized with different methods are presented in Fig. 4a and b, respectively. For all Co_3O_4 catalysts, irrespective of synthesis methods, the prominent peak of $Co2p_{3/2}$ level is deconvoluted into two peaks centered in a range of 779.3–779.4 and 780.05–780.35 eV attributed to Co^{3+} $2p_{3/2}$ and Co^{2+} $2p_{3/2}$ configuration [24]. The peaks corresponding to other spin-orbit component ($2p_{1/2}$) appear at 794.35–794.45 eV and 795.35–795.7 eV and are assigned to Co^{3+} $2p_{1/2}$ and Co^{2+} $2p_{1/2}$ configurations respectively [24]. Shake-up peaks of Co_3O_4 phase are also observed at 789 eV and 803.8 eV [25]. The exact oxidation state of Co can be determined

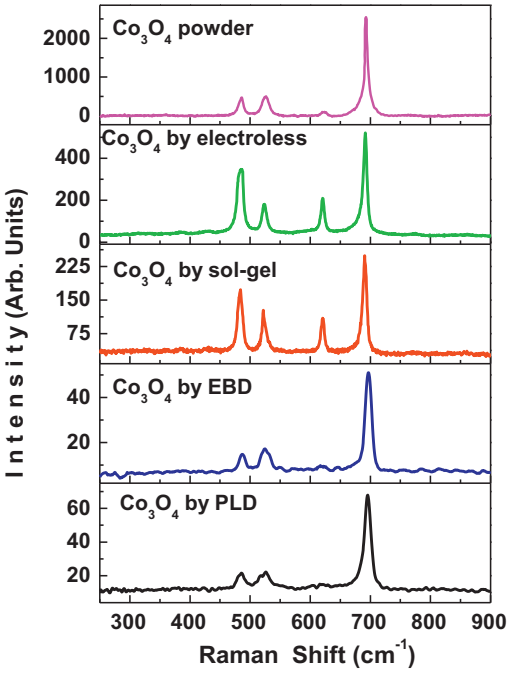

Fig. 3. Raman spectra of Co_3O_4 catalyst powder and coatings synthesized by PLD, EBD, sol–gel, and electroless deposition.

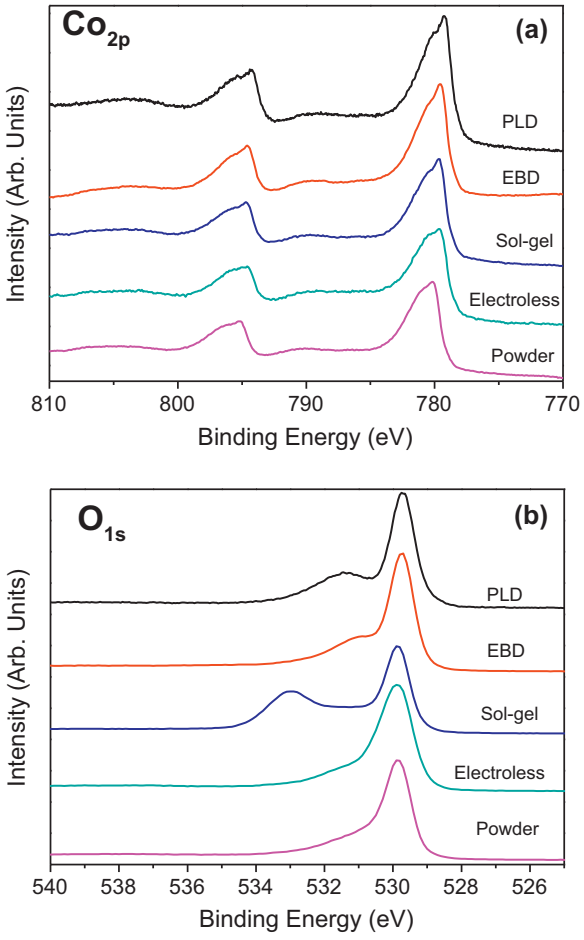

Fig. 4. X-ray photoelectron spectra of: (a) Co_{2p} and (b) O_{1s} core levels of Co_3O_4 catalyst powder and coatings synthesized by PLD, EBD, sol–gel, and electroless deposition.

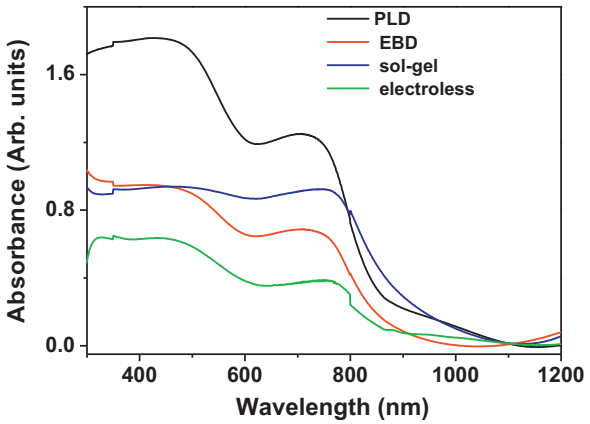

Fig. 5. UV–vis absorption spectra of Co_3O_4 coatings synthesized by different methods.

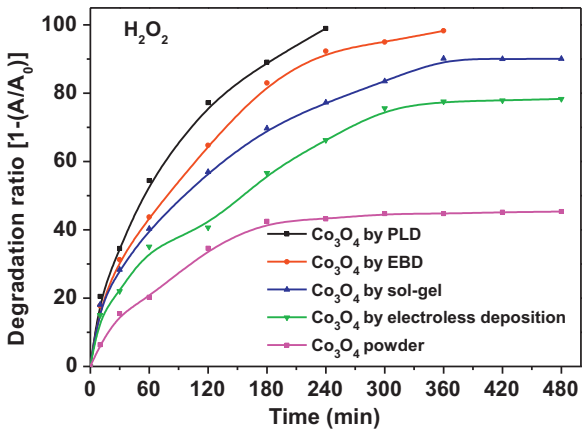

Fig. 6. Time dependent photocatalytic degradation ratio of MB solution in presence of H_2O_2 and visible light using Co_3O_4 catalyst powder and coatings prepared by PLD, EBD, sol–gel, and electroless deposition.

from spin–orbit splitting of the Co 2p peaks (ΔE) [26]. The energy difference of ~15.1 eV is measured between the main peak of Co $2p_{3/2}$ and the main peak of Co $2p_{1/2}$ which represents the characteristic of Co_3O_4 phase and in good agreement with the literature data [27]. Thus XPS confirms that all catalysts possess the Co_3O_4 spinel structure. The O 1s core level (Fig. 4b) is related to the peak at about 529.4 eV with a shoulder close to 531.1 eV corresponding to oxygen in the Co_3O_4 crystal lattice and to –OH (hydroxyl) attached to Co, respectively [24]. These peak positions are in well agreement with that reported for Co_3O_4 network. The presence of hydroxyl group on the catalyst surface is due to our ex situ experimental conditions.

Fig. 5 shows the optical absorption spectra of Co_3O_4 coatings synthesized by different methods on glass substrate. Two absorption peaks are observed at $\lambda \sim 720$ nm and $\lambda \sim 500$ nm that are assigned to ligand–metal charge transfer of O(II) → Co(III) and O(II) → Co(II), respectively [28]. These transitions confirm the existence of spinel Co_3O_4 phase [29]. However, the total absorption in visible range is significantly higher for PLD deposited Co_3O_4 coating as compared to the other Co_3O_4 coatings. Optical band gap was estimated by Tauc equation by plotting $(\alpha h\upsilon)^2$ vs $(h\upsilon)$ (figure not shown). The intercept of the straight line portion gives the band gap values which are listed in Table 2. For all the Co_3O_4 coatings the absorption edge values are in the range of 1.4–1.6 (E_{g1}) for lower energy side region and 1.8–2.2 (E_{g2}) for higher energy side region. These values are in good agreement with the reported Co_3O_4 band structure. However, E_{g1} is mainly assigned to the onset of O(II) → Co(III) excitation while E_{g2} is associated to the interband transition indicated as true band gap [28]. E_{g2} is blue shifted for the Co_3O_4 coating prepared with PLD as compared to other Co_3O_4 coatings. This shift can be due to quantum size effect created by the Co_3O_4 NPs on the surface of the PLD deposited coatings. Thus the evaluated optical properties confirm the nanocrystalline structure of Co_3O_4 coatings which might contribute to the better visible light absorption.

The photocatalytic activity of all the Co_3O_4 catalysts was tested by examining the degradation of MB dye solution as a function of time. The decrease of relative concentration of the MB dye was estimated by measuring the relative intensity of the peak at 664 nm from the optical absorbance spectra. The degree of discoloration of the MB solution was expressed in the form of degradation ratio $(1 - [A/A_0])$ where A_0 is the absorbance at $t = 0$ and A is the absorbance at given reaction time. In our past work [5], several experiments were carried out to degrade MB dye solution in presence or absence of light and with or without oxidant or catalyst. The degradation of dye was achieved in presence of visible light only when both oxidant (H_2O_2) and catalyst (Co_3O_4 coating) are present together, thus proving that dye is decolorized by photo Fenton reaction. Fig. 6 shows the rate of degradation of MB dye in presence of light and H_2O_2 using Co_3O_4 powder and coatings deposited with different methods. For comparison exactly the same weight (1.2 mg) was used for each catalyst. The reaction with Co_3O_4 NPs coating is completely heterogeneous since the previous reports show that the cobalt ions (Co^{2+}) leaching from heterogeneous Co_3O_4 and supported on TiO_2, MgO and Al_2O_3 catalyst usually is less than 1% even in acidic solutions [30,31]. Thus we also expect that negligible amount of cobalt ions will be leached in our case since low concentration of catalyst (1.2 mg) is used in the reaction. Co_3O_4 coatings synthesized with physical method such as PLD and EBD on glass substrate were able to completely photodegrade (99%) the MB dye solution: clear solution is obtained after 4 and 6 h irradiation, respectively. With Co_3O_4 coatings synthesized by chemical methods, even after 8 h the photo-degradation activity reaches 90% for sol–gel and 76% for electroless deposited coatings. Similarly, chemically synthesized powder shows only 45% photo-degradation activity after 8 h. There was no significant change in the decoloration of MB dye with further irradiation time for these chemically prepared Co_3O_4 catalysts. Maximum degradation rate was obtained with PLD deposited coatings. After 4 h, the PLD deposited Co_3O_4 coating was able to completely degrade the MB dye while for EBD, sol–gel and electroless prepared Co_3O_4 coatings, the photo-degradation activity was 92%, 77%, and 60%, respectively. All the Co_3O_4 coatings, irrespectively of preparation methods, show higher photo-degradation activity as compared to the Co_3O_4 powder. Although electroless deposited coating shows similar morphology and structural properties as that of powder, the degradation activity is almost 2 times higher than that of powder sample. This behavior is mainly attributed to the NPs agglomeration caused during the reaction course for the powder samples. This problem is solved using the catalyst in form of coating. In addition, the coating has the important advantage of being easily recovered and reused thus possibly operating as ON/OFF switch for the catalytic reaction.

Table 2
Band gap values as estimated from Tauc plot of $(\alpha h\upsilon)^2$ vs $(h\upsilon)$ for Co_3O_4 coatings synthesized by different methods.

Co_3O_4 catalyst coatings preparation technique	E_{g1} (eV)	E_{g2} (eV)
PLD	1.55	2.16
EBD	1.51	1.93
Sol–gel	1.43	1.83
Electroless deposition	1.53	1.96

The enhanced activity for the PLD deposited Co_3O_4 coating is mainly attributed to the following features established by the above characterizations:

1. Presence of spherical NPs on the catalyst surface with average size of about 18 nm.
2. NPs are well separated and embedded on the catalyst surface with size distribution in a narrow range ($\sigma = 3$ nm).
3. Presence of mixed amorphous-nanocrystalline phase.
4. Better absorption of light in visible region of the spectrum.

Spherical NPs with average size of 18 nm and narrow size distribution ($\sigma = 3$ nm) provide large number of surface active atoms with respect to bulk and just this condition is most favorable for surface-based catalytic reaction. These NPs are partially embedded on the catalyst surface thus forming 3D structure with higher surface area than the flat coating. In addition, unlike powder catalyst, the embedded NPs are stabilized against coarsening during the catalytic reaction. Mixed amorphous-nanocrystalline phase is composed of large amount of grain boundaries with width of 0.5–1.0 nm that can be considered as linear defects containing atoms with lower coordination number as compared to atoms in the ideal bulk crystallites. Thus, these grain-boundaries regions are highly catalytic active sites with basic, acidic or redox functionality [32]. Generally the Co_3O_4 catalysts operate through photo-Fenton reaction where Co^{2+} on the surface of catalyst reacts with H_2O_2 to produce $OH^{\bullet}$ radical and Co^{3+} ions [5]. However, light is necessary to regenerate Co^{2+} ions by reduction of Co^{3+} with the ligands (L) present in the solution (possible ligands are: OH^-, HO_2^-, carboxylates, etc.). Thus, the increased visible light absorption helps to accelerate the reduction of Co^{3+} to Co^{2+} for the PLD deposited Co_3O_4 coating. Without light, only 10% of MB dye is degraded in presence of Co_3O_4 and H_2O_2. All previous reasons are expected to enhance the photocatalytic activity of the PLD deposited Co_3O_4 coating.

The total light absorption in the visible range is lower for the EBD prepared Co_3O_4 coating and this might be the reason for slight decrease in the photo-degradation activity as compared to the PLD prepared coating. The granular morphology of the EBD coating with average size (27 nm) higher than that of the NPs synthesized by PLD may also affect the photo-degradation activity. However, these grains have narrow size distribution with amorphous-nanocrystalline phase thus providing favorable condition for the catalytic reaction. The previous features of the EBD deposited coatings explain why their photocatalytic activity is better than that of the chemically prepared (sol–gel and electroless) Co_3O_4 coatings. Indeed, in case of sol–gel deposited coating, even though the spherical NPs have smaller average size (20 nm) and are present on the surface, they are prone to agglomeration leading to lower activity than physically synthesized coatings. Electroless deposited Co_3O_4 coating shows the lowest degradation activity and is not able to decolorize the MB dye. NPs with irregular shape, having relatively large average size and broad size distribution are the main drawbacks of this coating. Besides, the absorption of the visible light is lowest and the coating is well crystallized: these are additional reasons behind the low activity of the electroless deposited Co_3O_4 coating.

In the past, several investigations showed that peroxymonosulfate (PMS) reagent, commonly known as oxone produces sulfate radicals that are oxidizing species which are more efficient on degradation of organic molecules as compared to other oxidants [6–8]. The active component of Oxone is $KHSO_5$. It was proved that Co^{2+} ion is the best catalyst for the activation of PMS and also cost effective than Co^{2+}/H_2O_2 system due to the requirement of very low concentration of oxone. Thus, in order to investigate the efficiency of Co_3O_4 NPs assembled coatings in sulfate radical generation, the MB dye degradation was studied in presence of oxone (Fig. 7). Although the concentration of oxone (0.5 mM) was very small as compared to H_2O_2 (100 mM) the photo-degradation of MB dye solution is much faster than H_2O_2 and Co_3O_4 catalyst irrespective of synthesis method. This is attributed to the standard reduction potential of sulphate radical (2.6–3.1 V) higher than that of $OH^{\bullet}$ radical (1.8–2.7 V) [7]. While all Co_3O_4 catalysts were able to completely decolorize the dye solution, PLD synthesized Co_3O_4 coating shows the highest degradation rate as compared to other coatings. For PLD coating, the time required for completely decolorize the MB dye is 8 min while for EBD, sol–gel, and electroless deposited coatings the required times are 22, 35 ad 60 min, respectively. In Co_3O_4 catalyst, the Co^{2+} ions activate the oxone ($2KHSO_5$, $KHSO_4$, K_2SO_4) molecule to produce sulfate radical and Co^{3+} ions accordingly to equations below [11]:

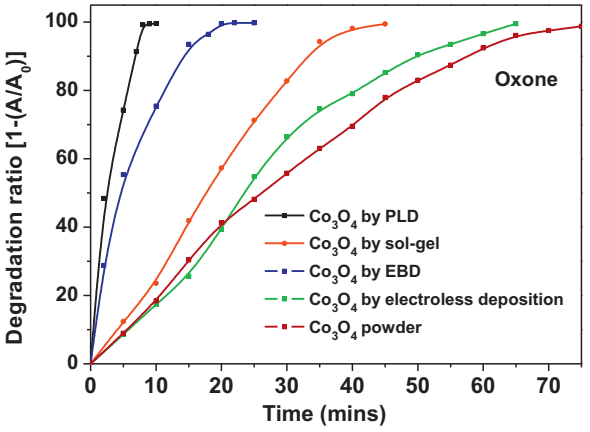

Fig. 7. Time dependent photocatalytic degradation ratio of MB solution in presence of oxone and visible light using Co_3O_4 catalyst powder and coatings prepared by PLD, EBD, sol–gel, and electroless deposition.

$$Co^{2+} + HSO_5^- \rightarrow Co^{3+} + SO_4^- + OH^- \quad (1)$$

$$SO_4^- + \text{dye} \rightarrow CO_2 + H_2O + \text{inorganic product} \quad (2)$$

$$Co^{3+} - L + h\nu \rightarrow Co^{2+} + L \quad (3)$$

The sulfate radical oxidizes the organic pollutants into CO_2, H_2O and other inorganic product, and Co^{3+} ion is reduced to Co^{2+} ion with the ligands (L), present in the solution, by absorption of light. Thus the higher absorption of visible light by the PLD synthesized Co_3O_4 coating is also accountable for the higher photo-degradation activity of MB dye. The powder Co_3O_4 catalyst shows lower activity than all the Co_3O_4 coatings irrespective of the synthesis method.

4. Conclusions

We compared the photo-catalytic efficiency of Co_3O_4 NPs assembled thin coatings synthesized by physical (PLD and EBD) and chemical (sol–gel and electroless) techniques for methylene blue dye degradation. The catalytic activity of these Co_3O_4 heterogeneous catalyst coatings occurs via photo Fenton reaction in presence of H_2O_2 or oxone oxidants. The Co_3O_4 NPs synthesized by PLD showed the best photo-degradation rate. The grains of the EBD coating have average size (27 nm) higher than that of the NPs synthesized by PLD (18 nm). Both PLD and EBD coatings have mixed amorphous-nanocrystalline structure that provides favorable conditions for the catalytic reaction. In case of sol–gel deposited coating, the spherical NPs have average size (20 nm) smaller than that of the EBD coating but they are prone to agglomeration leading to lower activity than physically synthesized coatings. Electroless deposited Co_3O_4 coating shows the lowest degradation activity and is not able to fully decolorize the MB dye. Here, the main

drawbacks are NPs having relatively large average size and broad size distribution along with the lowest absorption of the visible light.

Acknowledgements

We acknowledge C. Armellini for the support in the XRD analysis, E. Moser for support in the Raman measurements, and G. Scarduelli for XPS measurements. The research activity is partially supported by 7th UE research programme (Marie Curie Action, PATCOFUND).

References

[1] G.P. Anipsitakis, E. Stathatos, D.D. Dionysiou, Journal of Physical Chemistry B 109 (2005) 13052–13055.
[2] W.Y. Li, L.N. Xu, J. Chen, Advanced Functional Materials 15 (2005) 851.
[3] L. Cao, M. Lu, H.L. Li, Journal of the Electrochemical Society 152 (2005) A871.
[4] A. Mills, S.L. Hunte, Journal of Photochemistry and Photobiology A 108 (1997) 1–17.
[5] T. Warang, N. Patel, A. Santini, N. Bazzanella, A. Kale, A. Miotello, Applied Catalysis A-General 423–424 (2012) 21–27.
[6] N.N. Binitha, P.V. Suraja, Z. Yaakob, M.R. Resmi, P.P. Silija, Journal of Sol-Gel Science and Technology 53 (2010) 466–469.
[7] S.K. Ling, S. Wang, Y. Peng, Journal of Hazardous Materials 178 (2010) 385–389.
[8] J. Fernandez, P. Muruthamuthu, A. Renken, J. Kiwi, Applied Catalysis B 49 (2004) 207–215.
[9] V. Pralong, J.B. Leriche, B. Beaudoin, E. Naudin, M. Morcrette, J.M. Tarascon, Solid State Ionics 166 (2004) 295–305.
[10] Y. Wang, Z.W. Fu, Q.Z. Qin, Thin Solid Films 441 (2003) 19–24.
[11] P. Raja, M. Bensimon, U. Klehm, P. Albers, D. Laub, L. Kiwi-Minsker, A. Renken, J. Kiwi, Journal of Photochemistry and Photobiology A: Chemistry 187 (2007) 332–338.
[12] S. Laureti, E. Agostinelli, G. Scavia, G. Varvaro, V. Rossi Albertini, A. Generosi, B. Paci, A. Mezzi, S. Kaciulis, Applied Surface Science 254 (2008) 5111–5115.
[13] J. Wöllenstein, M. Burgmair, G. Plescher, T. Sulima, J. Hildenbrand, H. Böttner, I. Eisele, Sensors and Actuators B 93 (2003) 442–448.
[14] V. Balouria, S. Samanta, A. Singh, A.K. Debnath, A. Mahajan, R.K. Bedi, D.K. Aswal, S.K. Gupta, Sensors and Actuators B: Chemical 176 (2013) 38–45.
[15] M.E. Donders, H.C.M. Knoops, M.C.M. van, W.M.M. Kessels, P.H.L. Notten, Journal of the Electrochemical Society 158 (4) (2011) G92–G96.
[16] C. Guyon, A. Barkallah, F. Rousseau, K. Giffard, D. Morvan, M. Tatoulian, Surface & Coatings Technology 206 (2011) 1673–1679.
[17] F. Švegl, B. Orel, I. Grabec-Švegl, V. Kaucic, Electrochimica Acta 45 (2000) 4359–4371.
[18] Katalin Sinkó, Géza Szabó, Miklós Zrínyi, Journal of Nanoscience and Nanotechnology 11 (2011) 1–9.
[19] M. Bonelli, C. Cestari, A. Miotello, Measurement Science and Technology 10 (1999) N27–N30.
[20] A. Miotello, R. Kelly, Applied Physics Letters 67 (1995) 3535–3537.
[21] L.V. Zhigilei, Z. Lin, D.S. Ivanov, Journal of Physical Chemistry C 113 (2009) 11892–11906.
[22] M.M. Thackeray, W.I.F. David, J.B. Goodenough, Materials Research Bulletin 17 (1982) 785–793.
[23] V.G. Hadjiev, M.N. Iliev, I.V. Vergilov, Journal of Physics C-Solid State Physics 21 (1988) L199–L201.
[24] NIST data base for XPS core levels.
[25] S. Angelov, D. Mechandjiev, B. Piperopv, V. Zarkov, A. Terlecki-Baricevic, D. Jovanovic, Z. Jovanovic, Applied Catalysis 16 (1985) 431–437.
[26] H. Wang, H. Zhu, Z. Qin, F. Liang, G. Wang, J. Wang, Journal of Catalysis 264 (2009) 154–162.
[27] C.D. Wanger, W.M. Riggs, L.E. Davis, J.F. Moulder, G.E. Muilenberg, Handbook of X-ray Photoelectron Spectroscopy, Perkin-Elmer, Eden Prairie, 1978.
[28] R. Xu, J. Wang, Q. Li, G. Sun, E. Wang, S. Li, J. Gu, M. Ju, Journal of Solid State Chemistry 182 (2009) 3177–3182.
[29] P.S. Patil, L.D. Kadam, C.D. Lokhande, Thin Solid Films 272 (1996) 29–32.
[30] W. Zhang, H.L. Tay, S.S. Lim, Y. Wang, Z. Zhong, R. Xu, Applied Catalysis B: Environmental 95 (2010) 93–99.
[31] Q.J.H. Choi, V.J. Chen, D.D. Dionysiou, Applied Catalysis B: Environmental 77 (2008) 300–307.
[32] J. Tyczkowski, R. Kapica, J. Łojewska, Thin Solid Films 515 (2007) 6590–6595.